



Published in final edited form as:

J Comp Neurol. 2019 May 01; 527(7): 1278–1289. doi:10.1002/cne.24628.

Selective Cre-mediated gene deletion identifies connexin 43 as the main connexin channel supporting olfactory ensheathing cell networks

Ana Paula Piantanida^{1,2,a,b}, Luis Ernesto Acosta^{1,2,a}, Lucila Brocardo^{1,2}, Claudia Capurro^{1,2}, Charles A. Greer^{3,4}, and Lorena Rela^{1,2,c}

¹CONICET, Instituto de Fisiología y Biofísica Bernardo Houssay (IFIBIO), Neurociencia de Sistemas, C1121ABG, Buenos Aires, Argentina.

²Universidad de Buenos Aires, Instituto de Fisiología y Biofísica Bernardo Houssay (IFIBIO), Neurociencia de Sistemas, C1121ABG, Buenos Aires, Argentina.

³Yale University School of Medicine, Department of Neuroscience, New Haven, CT 06520.

⁴Yale University School of Medicine, Department of Neurosurgery, New Haven, CT 06520.

Abstract

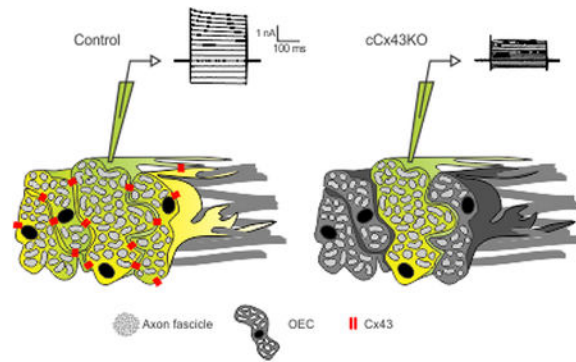
Many functions of glial cells depend on the formation of selective glial networks mediated by gap junctions formed by members of the connexin family. Olfactory ensheathing cells (OECs) are specialized glia associated with olfactory sensory neuron axons. Like other glia, they form selective networks, however, the connexins that support OEC connectivity *in vivo* have not been identified. We used an *in vivo* mouse model to selectively delete candidate connexin genes with temporal control from OECs and address the physiological consequences. Using this model we effectively abolished the expression of connexin 43 (Cx43) in OECs in both juvenile and adult mice. Cx43-deleted OECs exhibited features consistent with the loss of gap junctions including reduced membrane conductance, largely reduced sensitivity to the gap junction blocker meclofenamic acid and loss of dye coupling. This indicates that Cx43, a typically astrocytic connexin, is the main connexin forming functional channels in OECs. Despite these changes in functional properties, the deletion of Cx43 did not alter the density of OECs. The strategy used here may prove useful to delete other candidate genes to better understand the functional roles of OECs *in vivo*.

Graphical Abstract

^cCorresponding autor. Address: IFIBIO Houssay CONICET-UBA, University of Buenos Aires School of Medicine, Calle Paraguay 2155, 7mo piso, (1121) CABA, Argentina, Telephone: +54 11 5285 2800 ext 53309, lorena.rela@fmed.uba.ar.

^aAPP and LEA should be considered joint first author.

^bPresent address: Instituto de Virología, CICVyA, Instituto Nacional de Tecnología Agropecuaria (INTA), Los Reseros y Nicolás Repetto S/N, Castelar, 1712 Buenos Aires, Argentina.



Inducible PLP-Cre mice express Cre recombinase in olfactory ensheathing cells with temporal control, sparing astrocytes.

Cx43 mediates sensitivity to meclofenamic acid and gap junction coupling in olfactory ensheathing cells.

Olfactory ensheathing cells are viable after Cx43 deletion.

Keywords

olfactory ensheathing cells; connexin 43; gap junctions; proteolipid protein; Cre recombinase; RRID:IMSR_JAX:005975; RRID:IMSR_JAX:007914; RRID:IMSR_JAX:008039; RRID: AB_2533973; RRID: AB_2110187; RRID: AB_2533979; RRID: AB_10000325; RRID: AB_561049; RRID: AB_2576217; RRID: AB_141596

Introduction

Olfactory ensheathing cells (OECs) are specialized glial cells with neurotrophic properties (Kafitz & Greer, 1999; Lipson, Widenfalk, Lindqvist, Ebendal, & Olson, 2003; Nakhjavan-Shahraki et al., 2018; Runyan & Phelps, 2009) that are associated with olfactory sensory neurons (Doucette, 1991, 1993) and constitute a heterogeneous cell population in terms of molecular markers (W. Au, Treloar, & Greer, 2002; Honoré et al., 2012; Murthy, Bocking, Verginelli, & Stifani, 2014), cell adhesion (Windus et al., 2010) and physiological properties (Rela, Piantanida, Bordey, & Greer, 2015; Thyssen et al., 2013). A single molecular marker for OECs has not been yet identified. Rather, they express a unique combination of glial markers such as brain lipid-binding protein (BLBP) typically identified with radial glia (Feng, Hatten, & Heintz, 1994; Murdoch & Roskams, 2008; Rela, Bordey, & Greer, 2010), S100B expressed by Schwann cells and subpopulations of astrocytes (E Au & Roskams, 2003; Puckett et al., 1987; Rela et al., 2010) and DM-20, a splice variant of the proteolipid protein (PLP) gene also expressed by oligodendrocytes and Schwann cells (Dickinson et al., 1997). The lack of a specific genetic marker for OECs has prevented the development of models for OEC manipulation with sufficient selectivity to address the physiological roles of candidate genes *in vivo*.

OECs express high levels of Cx43 and can form selective gap junction-connected networks (Rela et al., 2010; Rela et al., 2015). Other glial connexins like Cx26, Cx32, and Cx30 are

absent or found only at low levels in the OECs from the olfactory bulb (OB) (Rela et al., 2010; Roux, Benchenane, Rothstein, Bonvento, & Giaume, 2011). Cx43 is one of the main functional connexins expressed by astrocytes and together with Cx30 mediates the formation of gap junction-connected astrocytic networks (Wallraff et al., 2006). Extracellular potassium buffering and delivery of energy metabolites to neurons critically depend on the formation of astrocyte networks (Rouach, Koulakoff, Abudara, Willecke, & Giaume, 2008; Wallraff et al., 2006). Oligodendrocytes can form homotypic networks coupled by Cx32 and Cx47 and heterotypic gap junctions with astrocytic connexins (Cx30, Cx43 and Cx26), which are essential for myelin integrity and astrocyte survival (Lutz et al., 2009; Maglione et al., 2010; Magnotti, Goodenough, & Paul, 2011; Wasseff & Scherer, 2011). Cx32 is essential as well for auto-cellular junctions and myelin maintenance in Schwann cells and oligodendrocytes (Anzini et al., 1997; Sargiannidou et al., 2009). The contribution of Cx43 to OEC gap junction coupling and whether it is co-expressed with other glial connexins is not known.

Here we use an *in vivo* approach to delete coding sequences for Cx43 in mice that express a tamoxifen (Tx)-inducible form of Cre recombinase under regulatory sequences of PLP (PLP-CreER^T). This line targets OECs, oligodendrocytes and Schwann cells and spares astrocytes. Thus, the PLP-CreER^T line is useful for Cre-dependent inducible deletion of genes that are expressed by OECs. With this strategy we show that Cx43 is the main connexin underlying the physiological properties associated with gap junction coupling in OECs both in juvenile and adult mice.

Materials and Methods

Animals

To characterize the expression pattern of Cre recombinase in the PLP-CreER^T line (PLP-Cre, for simplicity), we used male and female PLP-Cre;Tom mice (*Mus musculus*) obtained by crossing heterozygous PLP-Cre [B6.Cg-Tg(Plp1-cre/ESR1)3.16Pop/J, Stock 5975, The Jackson Laboratories, RRID:IMSR_JAX:005975] (Doerflinger, Macklin, & Popko, 2003) and homozygous LSL-Tom mice [B6.Cg-Gt(ROSA)26Sor^{tm14(CAG-tdTomato)Hze/J}, stock 7914, The Jackson Laboratories, RRID:IMSR_JAX:007914] (Madisen et al., 2010) in which Cre-expressing cells are reported by the fluorescent protein tdTomato (Tom). For all other experiments, we used the second generation offspring of heterozygous PLP-Cre mice crossed with Cx43^{fllox} mice [B6.129S7-Gja1^{tm1Dlg/J}, Stock 8039, The Jackson Laboratories, RRID:IMSR_JAX:008039] (Liao, Day, Damon, & Duling, 2001). Juvenile and adult mice of both sexes were 2 weeks and 2 months old, respectively. Up to six mice were housed per cage with water and food ad libitum and 12:12 h light/dark cycle (lights on at 7:00 A.M.), and cared for in accordance with institutional and government regulations (IACUC of the School of Medicine, University of Buenos Aires, 2598/13 and SENASA, Argentina). Tx (Sigma-Aldrich) was dissolved 1:10 in sunflower oil (Sigma-Aldrich) from a 100 mg/ml stock prepared in ethanol. A daily dose of 50 mg/kg (juvenile) or 100 mg/kg (adults) was given (i.p.) for five consecutive days. Juvenile mice were treated from postnatal day 14 (P14) to P19 and adult mice were treated from P60 to P65. Neonate mice received a daily dose of 50 mg/kg for two consecutive days (P1-P2). Mice were anesthetized with chloral hydrate

before perfusion (600 mg/kg, i.p.) or decapitation to obtain acute brain slices (400 mg/kg, i.p.).

Acute slice preparation

Preparation of horizontal brain slices containing the OB was carried out as previously reported (Rela et al., 2010). Briefly, anesthetized mice were decapitated and the brain quickly removed and chilled (0–4 °C) in 95% O₂-5% CO₂-saturated sucrose-based artificial cerebrospinal fluid (ACSF) containing (in mM): 220 Sucrose, 2.5 KCl, 1 CaCl₂, 6 MgCl₂, 1.25 NaH₂PO₄, 26 NaHCO₃ and 10 glucose. The brain was glued ventrally with cyanoacrylate glue to the stage of a vibratome (Pelco T series 1000, Ted Pella) and 300 µm slices were cut in cold oxygenated sucrose-based ACSF. The slices were recovered at room temperature for a period of >1 hour in normal ACSF containing (in mM): 125 NaCl, 2.5 KCl, 2 CaCl₂, 1.1 MgCl₂, 1.25 NaH₂PO₄, 26 NaHCO₃ and 10 glucose, pH 7.4. After recovery, slices were placed in a flow-through chamber, held in position by a harp (Warner Instruments, Hamden, CT), and continuously superfused with oxygenated normal ACSF at room temperature.

Electrophysiological recordings and drug applications

Patch-clamp experiments were performed on an upright Nikon Eclipse E600FN microscope (Bioanalytica, Argentina) equipped with Nomarski phase-contrast, water-immersion and fluorescence optics (60×; numerical aperture, 0.8), and infra-red illumination. Cells were visually identified in the olfactory nerve layer (ONL) of the OB and were chosen such that they were not adjacent to blood vessels. Whole cell voltage-clamp recordings were obtained as previously described (Rela et al., 2010). Patch pipettes were pulled from thin-walled borosilicate glass (1.50 / 1.10 mm outside / inside diameters, respectively; BF150-110-10; Sutter Instrument, Novato, CA) on a P-97 puller (Sutter Instruments). Pipettes had resistances of 5–10 MΩ when filled with the following solution (in mM): 130 KCl, 0.25 CaCl₂, 4 MgCl₂, 5 ethylene glycol-bis-(aminoethyl ether)-*N,N,N',N'*-tetraacetic acid (EGTA), 10 N-2-hydroxyethylpiperazine-*N'*-2-ethanesulfonic acid (HEPES), 4 K₂ATP, 0.5 Na₂GTP; 10 phosphocreatine was added for recordings of adult OECs. The pH was adjusted to 7.3 with KOH. Osmolarity of the intracellular and extracellular solutions were 295–300 and 305–310 mOsm, respectively. The osmolarity was measured with a vapor pressure osmometer 5520 (Wescor, Logan, UT). Lucifer Yellow (dilithium salt, Invitrogen/Molecular Probes, 0.1%) was routinely added to the pipette solution in order to confirm the identity of OECs by their mesh-like structure and the presence of lacunae defined by fine processes (Rela et al., 2010). Recordings were performed using an Axopatch 1D amplifier (Molecular Devices, Sunnyvale, CA). Current signals were low-pass filtered at 1 kHz and digitized online at 10 kHz using a Digidata 1322A digitizing board (Molecular Devices) interfaced with a computer system. Data acquisition, storage, and analysis were done using PClamp version 9.2 (Molecular Devices). Recordings were performed from a holding potential of –80 mV, near the resting potential expected for OECs. For all measurements, capacitance and series resistance compensation (at least 60%) were used to minimize voltage errors. Settings were determined by compensating the transients of a small (10-mV), 50 ms hyperpolarizing voltage step. Leak conductance was not subtracted. Meclofenamic acid (MFA, 100 µM), was diluted in ACSF from a 25 mM stock prepared with molecular grade

H₂O, and applied through the perfusion system at a constant rate of 3 ml/min. Chemicals were purchased from Sigma-Aldrich. (Argentina) and Baker (Chemical Center, Argentina), unless otherwise noted.

Analysis of physiological data

Cells considered for data analysis fulfilled the following criteria: access resistance (R_a) < 25 M Ω , variability of R_a < 20% throughout the full recording and resting membrane potential (V_r) between -90 and -70 mV. R_a was estimated from the uncompensated transient capacitive current peak evoked by a 50 ms, -10 mV pulse, averaging five traces, as $V / I = R_a$. Resting potential (V_r) was determined as the voltage reading in zero-current mode. Input resistance (R_i) was calculated from the current at steady-state elicited by a -20 mV, 400 ms voltage step using Ohm's law. Whole-cell current amplitudes were measured at the end of voltage pulses. MFA-sensitive currents were calculated as the subtraction trace by trace of total currents in the presence of MFA from total currents in control conditions, using Clampfit software (Molecular Devices, Sunnyvale, CA).

Dye-coupling

OECs were recorded as before in OB slices from 2–3 week-old mice and filled with lucifer yellow (0.1%) added to the recording solution. These experiments used a Multiclamp 700B amplifier (Molecular Devices, Sunnyvale, CA) and a Nikon FN1 microscope equipped with Nomarski phase-contrast, water-immersion and fluorescence optics (40 \times ; numerical aperture, 0.8), and infra-red and LED epifluorescence illumination (Tolket, Argentina). After dye diffusion for 20 min the pipette was gently withdrawn and the slice was immediately fixed with 4% paraformaldehyde (PFA) in 0.1 M phosphate buffered saline (PBS) for 24 h at 4 °C, then transferred to PBS with 0.1% sodium azide and kept at 4 °C for 1 week at most. Slices were stained with DAPI (1 μ g/ml in PBS) for 30 min, washed in PBS for 10 min and mounted with Fluoro-Gel (EMS, Hartfield, PA) on glass coverslips.

Immunohistochemistry

The animals were anesthetized and intracardially perfused with phosphate-buffered saline (PBS) supplemented with 2 U/ml heparin and then with 4% PFA in PBS (pH 7.4). The brains were dissected, fixed with the same fixative for 2 h at 4 °C, rinsed in PBS, cryoprotected with 30% sucrose in PBS, embedded in cryosectioning medium (Cryoplast, Biopack, Argentina) and frozen. Coronal sections were cut at 25–30 μ m with a cryostat (Cryotome 620E, Thermo Scientific), mounted on gelatin-coated glass slides and kept until use at -20 °C. Slides were dried for 15 min on a hot plate at 60 °C, washed in PBS, blocked for 30 min at room temperature in blocking buffer containing 2% bovine serum albumin and 0.3% Triton X-100 (American Bioanalytical, Natick, MA) in PBS and incubated overnight at 4 °C with primary antibodies diluted in blocking buffer. Sections were then washed three times in 0.3% Triton X-100 in PBS for 5 min and subsequently incubated for 2 h at room temperature with secondary antibodies conjugated to Alexa Fluor (Invitrogen/Life Technologies, Grand Island, NY, Cat# A11034, RRID: AB_2576217 and Cat# A21127, RRID: AB_141596) and DAPI (1 μ g/ml), all diluted 1:1000 in blocking buffer. Sections were washed as above, rinsed in PBS, incubated with 1% sudan black (Mallinckrodt, Hobard, NY) in 70% methanol for 5 min at room temperature to reduce autofluorescence

from lipofuscin granules (Schnell, Staines, & Wessendorf, 1999), rinsed with 70% ethanol, washed 3 times with PBS for 5 min, mounted, and coverslipped.

Antibody characterization

All antibodies used are listed in Table 1. Two anti-Cx43 antibodies were used. The anti-Cx43 antibody raised in rabbit (RRID: AB_2533973, polyclonal) was used for micrographs shown in Figure 3 and detects a 43 kDa protein on western blots with samples of mouse brain, rat brain, and human smooth muscle cell extracts, without boiling. Reactivity with other connexin types has not been observed on western blots. Positive immunohistostaining is seen with mouse heart and thalamus tissue. Reactivity of this antibody with Cx43 is independent of phosphorylation status (Li, Ochalski, Hertzberg, & Nagy, 1998). This antibody was validated using immunohistochemistry in uterine tissue samples from conditional Cx43 knockout mice (Laws et al., 2008). The anti-Cx43 antibody raised in mouse (RRID: AB_2110187, monoclonal) was used for immunohistochemistry in juvenile and adult mice for data shown in Figure 3. This antibody detects a band of the appropriate size in HeLa cells transfected with an expression plasmid coding for Cx43 but not in the parental cell line (Gemel, Valiunas, Brink, & Beyer, 2004) and was validated in neonatal myocardiocyte cultures from Cx43-knockout mice (Beauchamp et al., 2012). The two anti-Cx43 antibodies are further validated with the data shown in Figure 3. The anti-Cx30 antibody (RRID: AB_2533979, polyclonal) shows a single band in western blots from rat and mouse brain (Nagy, Patel, Ochalski, & Stelmack, 1999), no labeling in the cochlea of Cx30 null mice and no cross-reaction with Cx26 in this tissue (Chang, Tang, Ahmad, Zhou, & Lin, 2008). The anti-BLBP antibody (RRID: AB_10000325, polyclonal) recognizes a single band at 15 kDa on western blots from neonate mouse brain tissue lysate (manufacturer's technical information). The anti-GFAP antibody (RRID: AB_561049, monoclonal) detects a 51-kDa band corresponding to GFAP in glioma extracts, with no reaction against cultured human RD cells that lack GFAP, and strong staining of astrocytes in rat cerebellum and spinal cord (Debus, Weber, & Osborn, 1983).

Image acquisition and analysis

Images were acquired with an Olympus FV1000/IX81 confocal microscope as single frames (all immunostaining, except GFAP) or z-stacks (dye-coupling and GFAP immunostaining) with 0.5–2 μm steps between optical sections, using an oil-immersion objective (40 \times ; numerical aperture, 1.3) and up to 2 \times digital zoom. At least two sections per animal, 300 μm apart, were imaged. Digital images were color balanced with Corel Photo-Paint 15.0 (Corel Corp., Ottawa, Canada). The composition of the images was not altered in any way.

Image analysis was performed with ImageJ (Schneider, Rasband, & Eliceiri, 2012). To characterize cells reported in PLP-Cre;Tom mice, nuclear profiles with a cross-sectional area of at least 10 μm^2 were counted manually with the multipoint selection tool in ImageJ and circular regions of interest (4 μm^2) were generated at the locations of each point. The average intensity of Tom was measured for all ROIs. A histogram with these values yielded a bimodal shape that was used to classify cells as Tom⁺ or Tom⁻ depending on whether their intensity was above or below the minimum between peaks, respectively. Cells were considered positive for BLBP when the average intensity of the corresponding ROI was

higher than the average intensity +2SD of at least 20 ROIs determined in an image of a negative control without primary antibody. This procedure was carried out for each OB layer independently. Cells were considered positive for GFAP when they showed clearly stained perinuclear ring and emerging processes. Comparable criteria were used to quantify cell density in all single-frame images. In image stacks corresponding to dye coupling experiments, nuclei were counted once at the slice showing the larger nuclear diameter, including fractional nuclei. Cells were considered coupled to the recorded cell if the dye intensity was higher than the average intensity +2SD, determined for cells from comparable images obtained after failed attempts of dye filling, when a cell was patched and filled, but the dye was not retained after fixing and processing.

The intensity profile of Cx43 immunoreactivity as a function of depth in the ONL was performed with the Plot Profile function in ImageJ software (NIH). Three plot profiles corresponding to randomly selected rectangular ROIs of 20 μm in width and length adjusted to the thickness of the ONL, oriented perpendicular to the glomerular layer surface were averaged for each image after the application of an automatic threshold (triangle algorithm in ImageJ).

Graphs and statistical analysis

All graphs and statistical analyses were done with Prism 6 (GraphPad, La Jolla, CA). Tests used for statistical comparisons can be found in the figure legends and text where data are mentioned.

Results

The PLP-Cre line is a useful driver for olfactory ensheathing cells

Genetic manipulation of OECs is a challenge because no single molecular marker distinguishes them from other glial types. Among a combination of glial markers, OECs express DM-20, a splice variant of the PLP gene. Because oligodendrocytes are not found associated with OSN axons, here we asked whether a PLP-Cre mouse line expressing a Tx-inducible form of Cre recombinase under regulatory sequences of the PLP gene, could serve as a driver line to produce Cre-Lox mediated deletion of candidate genes in OECs.

To characterize the Cre expression pattern of the PLP-Cre line we crossed it with a Cre-reporter line (LSL-Tom) and analyzed the location and identity of labeled cells in the OB of the offspring at the juvenile stage (Figure 1a–c). The large majority of the reported cells (Tom+) were located in the ONL of the OB ($87.1 \pm 0.4\%$), known to be largely populated by OECs (W. Au et al., 2002). In line with this, Tom+ cells in the ONL represented the large majority of cells in this layer (Figure 1d). A small proportion of Tom+ cells ($5.3 \pm 0.2\%$) were also localized to the outer aspect of the glomerular layer, and represented a reduced proportion of total cells in this layer (Figure 1d). Tom+ cells were found in deeper layers also at very low probability (Figure 1d). More than 80% of Tom+ cells in the ONL and more than half of Tom+ cells in the glomerular layer co-labelled with BLBP (Figure 2a–b), confirming their OEC identity. Furthermore, almost all BLBP+ cells expressed the Tom reporter (Figure 2b). None of the observed Tom-expressing cells co-labeled with the

astrocytic marker glial fibrillary acidic protein (GFAP) and none of the few identified GFAP+ cells were reported by Tom (Figure 2c). The few Tom+ cells located in the deeper layers of the OB did not express BLBP and are likely a subset of oligodendrocytes (Figure 2d) labeled during the window of exposure to Tx from P14 to P19, shortly after the onset of PLP expression in the deep OB layers, around P10 (Dickinson et al., 1997). These results show that the PLP-Cre line is efficient in producing Cre-Lox-mediated recombination in OECs and within the ONL is selective for OECs. The presence of Tom+;BLBP+ cells in the outer aspect of the glomerular layer confirms previous observations supporting that a subpopulation of OECs localize among periglomerular cells and send projections that form part of the glomerular neuropil (Rela et al., 2010; Valverde, Santacana, & Heredia, 1992).

Connexin 43 deletion is not compensated by connexin 30 nor compromises OEC viability

Among the putative mediators of OEC gap junction coupling, Cx43 emerges as the stronger candidate, as it is highly expressed in the ONL and colocalizes with OEC projections (Rela et al., 2010). To test the functional relevance of Cx43 in OECs we used the PLP-Cre line to drive Cre-Lox-mediated deletion of Cx43 coding sequences. For this, we used the second-generation offspring of PLP-Cre mice crossed with Cx43^{fllox} mice, treated with Tx or vehicle beginning at 2 weeks of age, and evaluated for Cx43 immunoreactivity in the ONL at 1 month of age (Figure 3a–c). Our previous reports showed that Cx43 labeling decays in the ONL as a function of distance from the glomerular layer interface with the ONL (Rela et al., 2015). This gradient was observed in Tx-treated Cx43^{fllox} and vehicle-treated PLP-Cre;Cx43^{fllox} mice; however, it disappeared in Tx-treated PLP-Cre;Cx43^{fllox} mice (Figure 3d), referred as Cx43 conditional knockout mice (cCx43KO) in the rest of the article. In average, Cx43 immunoreactivity was significantly reduced by 86 % across the ONL (average intensity was 11.6 ± 2.2 in controls and 1.6 ± 0.3 in cCx43KO mice; $p < 0.001$, Kruskal-Wallis test), validating the PLP-Cre line as a useful tool for Cre-Lox mediated deletion in OECs. In line with this result, Cx43 immunoreactivity remained unaltered in the glomerular layer of both control and cCx43KO mice (24.0 ± 9.8 average intensity in cCx43KO mice versus 13.9 ± 8.4 and 10.8 ± 2.9 average intensity in Tx-treated Cx43^{fllox} and vehicle-treated PLP-Cre;Cx43^{fllox} mice, respectively, $p = 0.494$, Kruskal-Wallis test).

Cx43 deletion in hippocampal astrocytes leads to upregulation of Cx30 (Rouach et al., 2008). To test whether this was the case for OECs, we evaluated Cx30 immunoreactivity in the ONL in cCx43KO mice and control littermates (Figure 3e–g). Cx30 was strongly expressed in leptomeninges (Nagy et al., 2001) but was virtually absent elsewhere in the ONL (Figure 3h). Cx30 immunoreactivity remained unaltered after Cx43 deletion both in the ONL (Figure 3h) and glomerular layer (8.7 ± 1.8 average intensity in cCx43KO mice versus 10.7 ± 5.9 and 25.7 ± 12.2 average intensity in Tx-treated Cx43^{fllox} and vehicle-treated PLP-Cre;Cx43^{fllox} mice, respectively, $p = 0.347$, Kruskal-Wallis test). Thus, Cx30 did not compensate for Cx43 deletion in juvenile mice.

To test whether an adequate control of Cx43 deletion could be achieved in adults, we treated PLP-Cre;Cx43^{fllox} mice and control littermates with Tx or vehicle at 2 months of age and evaluated Cx43 immunoreactivity one month later at 3 months of age. Cx43 expression levels in vehicle-treated PLP-Cre;Cx43^{fllox} mice were undistinguishable from levels

observed in Tx-treated Cx43^{flox} mice. In contrast, cCx43KO mice showed a 73 % reduction in Cx43 expression in the ONL (average intensity was 35.0 ± 6.2 in controls and 9.4 ± 2.1 in cCx43KO mice, $p=0.009$, Kruskal-Wallis test) (Figure 3i). As was the case for juvenile mice, Cx43 deletion was not compensated by an increase in Cx30 immunoreactivity in the ONL (Figure 3j) nor we detected Cx30 expression changes in the glomerular layer (27.1 ± 10.0 average intensity in cCx43KO mice versus 23.3 ± 5.2 and 19.8 ± 6.1 average intensity in Tx-treated Cx43^{flox} and vehicle-treated PLP-Cre;Cx43^{flox} mice, respectively, $p=0.609$, Kruskal-Wallis test). Likewise, we did not detect significant differences among adult groups in glomerular immunoreactivity for Cx43 (14.0 ± 3.8 average intensity in cCx43KO mice versus 4.5 ± 2.2 and 5.7 ± 4.5 average intensity in Tx-treated Cx43^{flox} and vehicle-treated PLP-Cre;Cx43^{flox} mice, respectively, $p=0.164$, Kruskal-Wallis test). Thus, the PLP-Cre line provides an adequate time control of Cx43 deletion in the adults, with no evidence of cumulative background recombination in non-induced mice (Figure 3i).

As connexin deletion can compromise the viability of glial cells (Magnotti et al., 2011), we addressed whether OEC density in the ONL was reduced one month after Tx induction of Cx43 deletion in adult mice. The abundance of OECs identified by BLBP labeling in the ONL was undistinguishable when comparing cCx43KO mice with control littermates (Figure 4a–c). Total cell density in the ONL was also unperturbed by the deletion (Figure 4d). These results strongly suggest that OECs display long term survival in the absence of Cx43 expression.

Connexin 43 is the main functional connexin channel in OECs

Previous reports indicate that gap junction coupling in OECs recorded from OB acute slices can be abolished by application of the connexin blocker meclofenamic acid (MFA) (Rela et al., 2010). In addition, OECs are variable in terms of membrane conductance and larger conductance correlates with higher MFA sensitivity (Rela et al., 2015). To test whether Cx43 is a molecular substrate for the MFA-sensitive conductance in OECs, we analyzed the sensitivity of OEC membrane currents to MFA in OB slices of adult cCx43KO mice and control littermates. Consistent with previous reports for juvenile mice (Rela et al., 2010), MFA reduced the amplitude of whole-cell membrane currents by $68 \pm 3 \%$ in OECs from adult control mice (Figure 5a,b). This effect was accompanied by a significant increase in input resistance ($122.0 \pm 26.7 \text{ M}\Omega$ in the presence of $100 \mu\text{M}$ MFA versus $36.5 \pm 3.8 \text{ M}\Omega$ in control ACSF, $p=0.0313$, Wilcoxon test, $n=5$). OEC whole-cell current amplitudes were 67% smaller in cCx43KO mice when compared with control mice (Figure 5a,b) and, as expected, the MFAsensitive current was largely reduced in cCx43KO mice compared with controls (Figure 5c). In addition, OECs from cCx43KO mice had higher input resistance than OECs in control mice when recorded in ACSF ($105.9 \pm 8.1 \text{ M}\Omega$ versus $59.4 \pm 8.1 \text{ M}\Omega$, Mann Whitney test, $p=0.0001$, $n=18-19$). Thus, the deletion of Cx43 from OECs mimics and occludes the effect of connexin blockade by MFA. OECs recorded from juvenile cCx43KO mice showed negligible MFA sensitivity (Figure 5d) and significantly higher input resistance than OECs from control mice ($121.1 \pm 11.9 \text{ M}\Omega$ versus $61.9 \pm 6.5 \text{ M}\Omega$, Mann Whitney test, $p=0.0002$, $n=15-11$). The morphology of recorded cells was characteristic of OECs (Figure 5e). Overall, these data indicates that Cx43 is the prevailing functional OEC connexin during the juvenile and adult stages.

Previous reports indicated that sensitivity to MFA correlates with dye coupling in OECs recorded from 2–3 week old mice (Rela et al., 2010). To test whether Cx43 mediates gap junction coupling in OECs we performed dye coupling experiments in acute OB slices from 2–3 week old cCx43KO mice and control littermates. To achieve an efficient Cx43 deletion at this age, Tx was administered at the early postnatal stage. When OECs were recorded from control mice, the recorded cell and neighboring cells were diffusely labeled by the dye (Figure 6). In contrast, most OECs recorded from cCx43KO mice were brightly labeled and no neighboring cells were labeled in most cases. Average dye intensity of cell bodies located within a radius of 50 μm from the filled cell was significantly lower in cCx43KO mice when compared with control mice (12.1 ± 2.5 versus 28.8 ± 4.2 expressed in arbitrary units from 0 to 255; $p=0.014$, significant effect of genotype in two-way ANOVA with genotype and distance as factors, Figure 6), indicating that OEC gap junction connectivity was limited in cCx43KO mice. In average, control OECs were dye coupled to significantly more neighboring cells than OECs from cCx43KO mice (11 ± 4 cells versus 3 ± 2 cells, $p=0.0429$, Mann Whitney test), matching previous reports indicating that lucifer yellow injections reveal dye coupling among small subgroups of OECs in juvenile mice (Rela et al., 2010). Overall, the data indicates that OEC gap junction connectivity is predominantly supported by Cx43.

Discussion

OECs have been characterized by the constellation of OEC markers they express and have been described as a heterogeneous cell population. OEC marker expression differs both between lamina propria and OB and between sublayers of the OB ONL. Available OEC reporters include the S100B-GFP and S100B-DsRed lines, which also label subpopulations of astrocytes and Schwann cells (Windus, Claxton, Allen, Key, & St John, 2007; Zuo et al., 2004) and the recently reported Cx43kiECFP line (Theofilas, Steinhäuser, Theis, & Derouiche, 2017), which also labels most astrocytes, meningeal cells, ependymal cells and some amacrine cell of the retina. Although the ONL is populated predominantly by OECs, these reporters also label a small number of astrocytes in the ONL. Our results show that the PLP-Cre;Tom line is as efficient as the S100-GFP line of mice in labeling OECs and is more selective because it spares astrocytes. An additional advantage of the PLP-Cre line is that it is temporally inducible and suitable for lineage analyses of OECs. OECs express predominantly the DM-20 splice variant of the PLP gene from embryonic day 14 (Dickinson et al., 1997) making the PLP-Cre line suitable for OEC tracing during development. Because the onset of expression of the PLP promoter is much earlier in OECs than in oligodendrocytes of the deep layers of the bulb, around postnatal day 10 (Dickinson et al., 1997), an additional advantage of the inducible PLP-Cre line is that OECs can be manipulated with little impact on oligodendrocytes, provided that Tx is administered early enough.

Knowledge about roles of OECs *in vivo* has emerged from non-inducible knock-down and null mice (E. Au et al., 2007; Ingram, Khankan, & Phelps, 2016; Murthy et al., 2014; Raucci, Tiong, & Wray, 2013). Selective genetic manipulation of OECs has been achieved using viral vectors in enriched OEC preparations to be used in transplants (Cao et al., 2004; Ruitenber et al., 2002). Immortalized OEC cell lines carrying transgenes have also been

generated (Plaza, Simón, Sierra, & Moreno-Flores, 2016; Reginensi et al., 2015). The cCx43KO mice used here are the first reported to knock-out candidate genes in OECs *in vivo* with high selectivity for OECs in the ONL and with temporal control. The lack of Cre-mediated Cx43 deletion in PLP-Cre;Cx43^{fllox} mice in the absence of Tx reveals that leakiness in Cre activity on the Cx43 locus remains undetectable, indicating an effective time control of the deletion. The PLP-Cre line is expected to delete the targeted genes of choice in oligodendrocytes and Schwann cells. The present data focused on the physiological roles of OECs in the ONL, devoid of oligodendrocytes and Schwann cells, thus it is unlikely that the observed effects derive from indirect effects mediated by these cell types.

Although OECs are often described as unique, it is noted that they are more similar to Schwann cells than to astrocytes (Ulrich et al., 2014). In terms of connexin expression, OECs show a partial astrocytic phenotype, as they express Cx43 but not Cx30. Connexins 26, 32, 37, 43, and 46 are expressed by OECs in culture (Barnett, Thompson, Lakatos, & Pitts, 2001). However, Cx26, another astrocytic connexin, and Cx32, typical of myelinating glia, are not detected in juvenile OECs *in situ* (Rela et al., 2010). Here we show that Cx43 expressed by OECs, is physiologically relevant to determine OEC membrane properties and dye coupling *in situ*, consistent with previous studies of ultrastructure showing that OEC gap junctions contain Cx43 (Rash et al., 2005). Our data also demonstrate that Cx43 is the primary OEC connexin explaining MFA sensitivity and dye coupling.

Besides a role in mediating gap junction coupling, Cx43 can function as unapposed non-junctional hemichannels to release gliotransmitters (Roux et al., 2015). The MFA-sensitive membrane current measured in OECs could be explained by gap junction block, as MFA has a direct blocking effect on OEC gap junction coupling (Rela et al., 2010). However we cannot rule out a contribution of Cx43 hemichannels to the total membrane current (Blinder, Pumplin, Paul, & Keller, 2003).

The genetic tool to manipulate OEC gene expression presented here opens a path to help identify key mechanisms in OEC biology with relevance for the design of OEC transplants as a therapeutic approach to promote recovery after neural damage.

Acknowledgements:

This work was supported in part by Secretaría de Ciencia, Tecnología e Innovación Productiva, Fondo para la Investigación Científica y Tecnológica (PICT-PRH 2009–0053, PICT 2011–1650, PICT 2014–1954), Universidad de Buenos Aires (UBACYT 20020100100562), and Consejo Nacional de Investigaciones Científicas y Técnicas (PIP 0332), Argentina, to LR and by NIH NIDCD DC013791 and DC015438 to CAG. We thank Paola Cardozo, Graciela Ortega, Jélica Unger, Verónica Risso, Analía López Díaz and Germán La Iacona, for technical assistance.

References

- Anzini P, Neuberg DH, Schachner M, Nelles E, Willecke K, Zielasek J, ... Martini R (1997). Structural abnormalities and deficient maintenance of peripheral nerve myelin in mice lacking the gap junction protein connexin 32. *J Neurosci*, 17(12), 4545–4551. [PubMed: 9169515]
- Au E, Richter MW, Vincent AJ, Tetzlaff W, Aebersold R, Sage EH, & Roskams AJ (2007). SPARC from olfactory ensheathing cells stimulates Schwann cells to promote neurite outgrowth and

enhances spinal cord repair. *J Neurosci*, 27(27), 7208–7221. doi:10.1523/JNEUROSCI.0509-07.2007 [PubMed: 17611274]

- Au E, & Roskams A (2003). Olfactory ensheathing cells of the lamina propria in vivo and in vitro. *Glia*, 41(3), 224–236. [PubMed: 12528178]
- Au W, Treloar H, & Greer C (2002). Sublaminar organization of the mouse olfactory bulb nerve layer. *J Comp Neurol*, 446(1), 68–80. [PubMed: 11920721]
- Barnett SC, Thompson RJ, Lakatos A, & Pitts J (2001). Gap junctional communication and connexin expression in cultured olfactory ensheathing cells. *J Neurosci Res*, 65(6), 520–528. doi:10.1002/jnr.1182 [pii] [PubMed: 11550220]
- Beauchamp P, Desplantez T, McCain ML, Li W, Asimaki A, Rigoli G, ... Kleber AG (2012). Electrical coupling and propagation in engineered ventricular myocardium with heterogeneous expression of connexin43. *Circ Res*, 110(11), 1445–1453. doi:10.1161/CIRCRESAHA.111.259705 [PubMed: 22518032]
- Blinder KJ, Pumplin DW, Paul DL, & Keller A (2003). Intercellular interactions in the mammalian olfactory nerve. *J Comp Neurol*, 466(2), 230–239. doi:10.1002/cne.10872 [PubMed: 14528450]
- Cao L, Liu L, Chen ZY, Wang LM, Ye JL, Qiu HY, ... He C (2004). Olfactory ensheathing cells genetically modified to secrete GDNF to promote spinal cord repair. *Brain*, 127(Pt 3), 535–549. doi:10.1093/brain/awh072 [PubMed: 14691064]
- Chang Q, Tang W, Ahmad S, Zhou B, & Lin X (2008). Gap junction mediated intercellular metabolite transfer in the cochlea is compromised in connexin30 null mice. *PLoS One*, 3(12), e4088. doi:10.1371/journal.pone.0004088 [PubMed: 19116647]
- Debus E, Weber K, & Osborn M (1983). Monoclonal antibodies specific for glial fibrillary acidic (GFA) protein and for each of the neurofilament triplet polypeptides. *Differentiation*, 25(2), 193–203. [PubMed: 6198232]
- Dickinson PJ, Griffiths IR, Barrie JM, Kyriakides E, Pollock GF, & Barnett SC (1997). Expression of the dm-20 isoform of the plp gene in olfactory nerve ensheathing cells: evidence from developmental studies. *J Neurocytol*, 26(3), 181–189. [PubMed: 9192285]
- Doerflinger N, Macklin W, & Popko B (2003). Inducible site-specific recombination in myelinating cells. *Genesis*, 35(1), 63–72. [PubMed: 12481300]
- Doucette R (1991). PNS-CNS transitional zone of the first cranial nerve. *J Comp Neurol*, 312(3), 451–466. doi:10.1002/cne.903120311 [PubMed: 1748741]
- Doucette R (1993). Glial cells in the nerve fiber layer of the main olfactory bulb of embryonic and adult mammals. *Microsc Res Tech*, 24(2), 113–130. doi:10.1002/jemt.1070240204 [PubMed: 8457724]
- Feng L, Hatten ME, & Heintz N (1994). Brain lipid-binding protein (BLBP): a novel signaling system in the developing mammalian CNS. *Neuron*, 12(4), 895–908. [PubMed: 8161459]
- Gemel J, Valiunas V, Brink PR, & Beyer EC (2004). Connexin43 and connexin26 form gap junctions, but not heteromeric channels in co-expressing cells. *J Cell Sci*, 117(Pt 12), 2469–2480. doi:10.1242/jcs.01084 [PubMed: 15128867]
- Honoré A, Le Corre S, Derambure C, Normand R, Duclos C, Boyer O, ... Guérout N (2012). Isolation, characterization, and genetic profiling of subpopulations of olfactory ensheathing cells from the olfactory bulb. *Glia*, 60(3), 404–413. doi:10.1002/glia.22274 [PubMed: 22161947]
- Ingram NT, Khankan RR, & Phelps PE (2016). Olfactory Ensheathing Cells Express $\alpha 7$ Integrin to Mediate Their Migration on Laminin. *PLoS One*, 11(4), e0153394. doi:10.1371/journal.pone.0153394 [PubMed: 27078717]
- Kafitz KW, & Greer CA (1999). Olfactory ensheathing cells promote neurite extension from embryonic olfactory receptor cells in vitro. *Glia*, 25(2), 99–110. doi:10.1002/(SICI)1098-1136(19990115)25:2<99::AID-GLIA1>3.0.CO;2-V [pii] [PubMed: 9890625]
- Laws MJ, Taylor RN, Sidell N, DeMayo FJ, Lydon JP, Gutstein DE, ... Bagchi IC (2008). Gap junction communication between uterine stromal cells plays a critical role in pregnancy-associated neovascularization and embryo survival. *Development*, 135(15), 2659–2668. doi:10.1242/dev.019810 [PubMed: 18599509]

- Li WE, Ochalski PA, Hertzberg EL, & Nagy JI (1998). Immunorecognition, ultrastructure and phosphorylation status of astrocytic gap junctions and connexin43 in rat brain after cerebral focal ischaemia. *Eur J Neurosci*, 10(7), 2444–2463. [PubMed: 9749772]
- Liao Y, Day K, Damon D, & Duling B (2001). Endothelial cell-specific knockout of connexin 43 causes hypotension and bradycardia in mice. *Proc Natl Acad Sci U S A*, 98(17), 9989–9994. [PubMed: 11481448]
- Lipson A, Widenfalk J, Lindqvist E, Ebendal T, & Olson L (2003). Neurotrophic properties of olfactory ensheathing glia. *Exp Neurol*, 180(2), 167–171. [PubMed: 12684030]
- Lutz SE, Zhao Y, Gulino M, Lee SC, Raine CS, & Brosnan CF (2009). Deletion of astrocyte connexins 43 and 30 leads to a dysmyelinating phenotype and hippocampal CA1 vacuolation. *J Neurosci*, 29(24), 7743–7752. doi:10.1523/JNEUROSCI.0341-09.2009 [PubMed: 19535586]
- Madisen L, Zwingman T, Sunkin S, Oh S, Zariwala H, Gu H, ... Zeng H (2010). A robust and high-throughput Cre reporting and characterization system for the whole mouse brain. *Nat Neurosci*, 13(1), 133–140. doi:10.1038/nn.2467 [pii] 10.1038/nn.2467 [PubMed: 20023653]
- Maglione M, Tress O, Haas B, Karram K, Trotter J, Willecke K, & Kettenmann H (2010). Oligodendrocytes in mouse corpus callosum are coupled via gap junction channels formed by connexin47 and connexin32. *Glia*, 58(9), 1104–1117. doi:10.1002/glia.20991 [PubMed: 20468052]
- Magnotti LM, Goodenough DA, & Paul DL (2011). Deletion of oligodendrocyte Cx32 and astrocyte Cx43 causes white matter vacuolation, astrocyte loss and early mortality. *Glia*, 59(7), 1064–1074. doi:10.1002/glia.21179 [PubMed: 21538560]
- Murdoch B, & Roskams AJ (2008). A novel embryonic nestin-expressing radial glia-like progenitor gives rise to zonally restricted olfactory and vomeronasal neurons. *J Neurosci*, 28(16), 4271–4282. doi:10.1523/JNEUROSCI.5566-07.2008 [PubMed: 18417707]
- Murthy M, Bocking S, Verginelli F, & Stifani S (2014). Transcription factor Runx1 inhibits proliferation and promotes developmental maturation in a selected population of inner olfactory nerve layer olfactory ensheathing cells. *Gene*, 540(2), 191–200. doi:10.1016/j.gene.2014.02.038 [PubMed: 24582971]
- Nagy JI, Li X, Rempel J, Stelmack G, Patel D, Staines WA, ... Rash JE (2001). Connexin26 in adult rodent central nervous system: demonstration at astrocytic gap junctions and colocalization with connexin30 and connexin43. *J Comp Neurol*, 441(4), 302–323. [PubMed: 11745652]
- Nagy JI, Patel D, Ochalski PA, & Stelmack GL (1999). Connexin30 in rodent, cat and human brain: selective expression in gray matter astrocytes, co-localization with connexin43 at gap junctions and late developmental appearance. *Neuroscience*, 88(2), 447–468. [PubMed: 10197766]
- Nakhjavan-Shahraki B, Yousefifard M, Rahimi-Movaghar V, Baikpour M, Nasirinezhad F, Safari S, ... Hosseini M (2018). Transplantation of olfactory ensheathing cells on functional recovery and neuropathic pain after spinal cord injury; systematic review and meta-analysis. *Sci Rep*, 8(1), 325. doi:10.1038/s41598-017-18754-4 [PubMed: 29321494]
- Plaza N, Simón D, Sierra J, & Moreno-Flores MT (2016). Transduction of an immortalized olfactory ensheathing glia cell line with the green fluorescent protein (GFP) gene: Evaluation of its neuroregenerative capacity as a proof of concept. *Neurosci Lett*, 612, 25–31. doi:10.1016/j.neulet.2015.12.001 [PubMed: 26655478]
- Puckett C, Hudson L, Ono K, Friedrich V, Benecke J, Dubois-Dalcq M, & Lazzarini RA (1987). Myelin-specific proteolipid protein is expressed in myelinating Schwann cells but is not incorporated into myelin sheaths. *J Neurosci Res*, 18(4), 511–518. doi:10.1002/jnr.490180402 [PubMed: 2449540]
- Rash J, Davidson K, Kamasawa N, Yasumura T, Kamasawa M, Zhang C, ... Nagy J (2005). Ultrastructural localization of connexins (Cx36, Cx43, Cx45), glutamate receptors and aquaporin4 in rodent olfactory mucosa, olfactory nerve and olfactory bulb. *J Neurocytol*, 34(3–5), 307–341. [PubMed: 16841170]
- Raucci F, Tiong JD, & Wray S (2013). P75 nerve growth factor receptors modulate development of GnRH neurons and olfactory ensheathing cells. *Front Neurosci*, 7, 262. doi:10.3389/fnins.2013.00262 [PubMed: 24409113]

- Reginensi D, Carulla P, Nocentini S, Seira O, Serra-Picamal X, Torres-Espín A, ... del Río JA (2015). Increased migration of olfactory ensheathing cells secreting the Nogo receptor ectodomain over inhibitory substrates and lesioned spinal cord. *Cell Mol Life Sci*, 72(14), 27192737. doi:10.1007/s00018-015-1869-3
- Rela L, Bordey A, & Greer CA (2010). Olfactory ensheathing cell membrane properties are shaped by connectivity. *Glia*, 58(6), 665–678. doi:10.1002/glia.20953 [PubMed: 19998494]
- Rela L, Piantanida AP, Bordey A, & Greer CA (2015). Voltage-dependent K(+) currents contribute to heterogeneity of olfactory ensheathing cells. *Glia*. doi:10.1002/glia.22834
- Rouach N, Koulakoff A, Abudara V, Willecke K, & Giaume C (2008). Astroglial metabolic networks sustain hippocampal synaptic transmission. *Science*, 322(5907), 1551–1555. [PubMed: 19056987]
- Roux L, Benchenane K, Rothstein JD, Bonvento G, & Giaume C (2011). Plasticity of astroglial networks in olfactory glomeruli. *Proc Natl Acad Sci U S A*, 108(45), 18442–18446. doi:10.1073/pnas.1107386108 [PubMed: 21997206]
- Roux L, Madar A, Lacroix MM, Yi C, Benchenane K, & Giaume C (2015). Astroglial Connexin 43 Hemichannels Modulate Olfactory Bulb Slow Oscillations. *J Neurosci*, 35(46), 15339–15352. doi:10.1523/JNEUROSCI.0861-15.2015 [PubMed: 26586821]
- Ruitenbergh MJ, Plant GW, Christensen CL, Blits B, Niclou SP, Harvey AR, ... Verhaagen J (2002). Viral vector-mediated gene expression in olfactory ensheathing glia implants in the lesioned rat spinal cord. *Gene Ther*, 9(2), 135–146. doi:10.1038/sj.gt.3301626 [PubMed: 11857072]
- Runyan SA, & Phelps PE (2009). Mouse olfactory ensheathing glia enhance axon outgrowth on a myelin substrate in vitro. *Exp Neurol*, 216(1), 95–104. doi:S0014-4886(08)00440-8 [pii] 10.1016/j.expneurol.2008.11.015 [PubMed: 19100263]
- Sargiannidou I, Vavlitou N, Aristodemou S, Hadjisavvas A, Kyriacou K, Scherer S, & Kleopa K (2009). Connexin32 mutations cause loss of function in Schwann cells and oligodendrocytes leading to PNS and CNS myelination defects. *J Neurosci*, 29(15), 4736–4749. [PubMed: 19369543]
- Schneider CA, Rasband WS, & Eliceiri KW (2012). NIH Image to ImageJ: 25 years of image analysis. *Nat Methods*, 9(7), 671–675. [PubMed: 22930834]
- Schnell SA, Staines WA, & Wessendorf MW (1999). Reduction of lipofuscin-like autofluorescence in fluorescently labeled tissue. *J Histochem Cytochem*, 47(6), 719–730. doi:10.1177/002215549904700601 [PubMed: 10330448]
- Theofilas P, Steinhäuser C, Theis M, & Derouiche A (2017). Morphological study of a connexin 43-GFP reporter mouse highlights glial heterogeneity, amacrine cells, and olfactory ensheathing cells. *J Neurosci Res*, 95(11), 2182–2194. doi:10.1002/jnr.24055 [PubMed: 28370142]
- Thyssen A, Stavermann M, Buddrus K, Doengi M, Ekberg JA, St John JA, ... Lohr C (2013). Spatial and developmental heterogeneity of calcium signaling in olfactory ensheathing cells. *Glia*, 61(3), 327–337. doi:10.1002/glia.22434 [PubMed: 23109369]
- Ulrich R, Imbschweiler I, Kalkuhl A, Lehmbecker A, Ziege S, Kegler K, ... Baumgärtner W (2014). Transcriptional profiling predicts overwhelming homology of Schwann cells, olfactory ensheathing cells, and Schwann cell-like glia. *Glia*, 62(10), 1559–1581. doi:10.1002/glia.22700 [PubMed: 24889922]
- Valverde F, Santacana M, & Heredia M (1992). Formation of an olfactory glomerulus: morphological aspects of development and organization. *Neuroscience*, 49(2), 255–275. [PubMed: 1436469]
- Wallraff A, Kohling R, Heinemann U, Theis M, Willecke K, & Steinhäuser C (2006). The impact of astrocytic gap junctional coupling on potassium buffering in the hippocampus. *J Neurosci*, 26(20), 5438–5447. doi:26/20/5438 [pii] 10.1523/JNEUROSCI.0037-06.2006 [PubMed: 16707796]
- Wasseff SK, & Scherer SS (2011). Cx32 and Cx47 mediate oligodendrocyte:astrocyte and oligodendrocyte:oligodendrocyte gap junction coupling. *Neurobiol Dis*, 42(3), 506–513. doi:10.1016/j.nbd.2011.03.003 [PubMed: 21396451]
- Windus LC, Claxton C, Allen CL, Key B, & St John JA (2007). Motile membrane protrusions regulate cell-cell adhesion and migration of olfactory ensheathing glia. *Glia*, 55(16), 1708–1719. doi:10.1002/glia.20586 [PubMed: 17893920]

- Windus LC, Lineburg KE, Scott SE, Claxton C, Mackay-Sim A, Key B, & St John JA (2010). Lamellipodia mediate the heterogeneity of central olfactory ensheathing cell interactions. *Cell Mol Life Sci*, 67(10), 1735–1750. doi:10.1007/s00018-010-0280-3 [PubMed: 20143249]
- Zuo Y, Lubischer J, Kang H, Tian L, Mikesh M, Marks A, ... Thompson W (2004). Fluorescent proteins expressed in mouse transgenic lines mark subsets of glia, neurons, macrophages, and dendritic cells for vital examination. *J Neurosci*, 24(49), 10999–11009. [PubMed: 15590915]

Author Manuscript

Author Manuscript

Author Manuscript

Author Manuscript

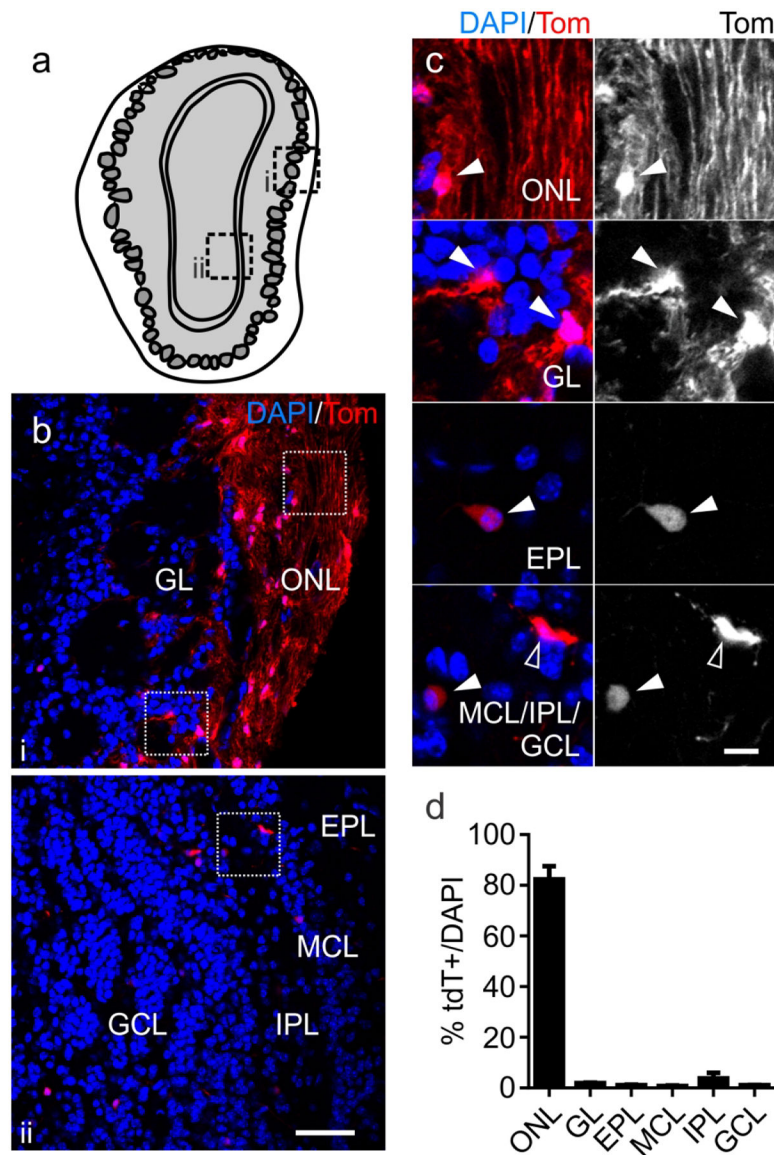


Figure 1. The PLP-Cre line directs Cre expression predominantly in cells in the ONL. (a) Schematic representation of an OB coronal section indicating the superficial (i) and deep (ii) regions imaged in b. (b) Representative images of coronal sections of the OB from 1-month-old PLP-Cre;Tom mice treated with Tx at 2 weeks of age (P14-P19). Expression of Tom and nuclear stain (DAPI) are shown in red and blue, respectively. Images labeled i-ii correspond to the approximate depths indicated in a. Scale bar: 50 μ m. ONL: olfactory nerve layer; GL: glomerular layer; EPL: external plexiform layer; MCL: mitral cell layer; IPL: internal plexiform layer; GCL: granule cell layer. Squared regions at the level of the ONL, GL and MCL/IPL/GCL are magnified in (c). (c) Details of cells labeled by Tom (red) in the different layers of the OB, indicated by arrowheads. The red channel is shown at the right in grayscale. The detail corresponding to the EPL is not shown in (b). Scale bar: 10 μ m. (d) Percent of nuclei colocalized with Tom in each OB layer (n=4 mice).

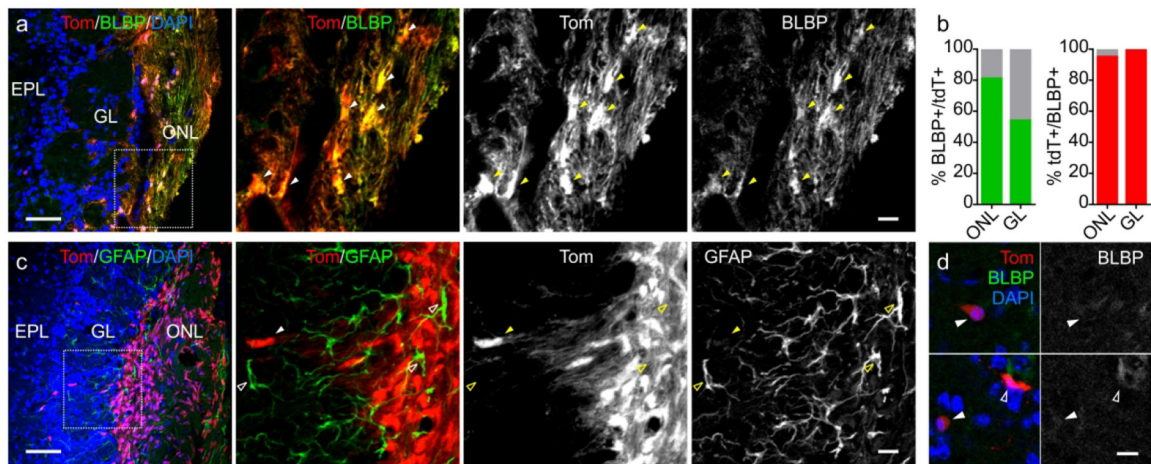


Figure 2. The PLP-Cre line efficiently and selectively targets olfactory ensheathing cells.

Representative images of coronal sections of the OB from 1-month-old PLP-Cre;Tom mice treated with Tx at 2 weeks of age (P14-P19). **(a)** Optical section showing expression of Tom, BLBP and nuclear stain (DAPI) in red, green and blue, respectively. The squared region is shown as combined or separate red and green channels at the right in a magnified scale, indicating Tom-labeled cells with arrowheads. Scale bar: 50 μm (left) and 10 μm (right). ONL: olfactory nerve layer; GL: glomerular layer; EPL: external plexiform layer. **(b)** Percent of Tom-labeled cells colocalized with the BLBP immunolabeling (left) and percent of BLBP immunolabeled cells colocalized with Tom expression (right) in the olfactory nerve and glomerular layers (n=3 mice). **(c)** Confocal stack (maximum projection) of images (7 optical sections at 0.5 μm between sections) showing expression of Tom, GFAP and nuclear stain (DAPI) in red, green and blue, respectively. The squared region is shown as combined or separate red and green channels at the right in a magnified scale. Scale bar: 50 μm (left) and 10 μm (right). Cells labeled by Tom expression are indicated with filled arrowheads and GFAP-immunolabeled cells are indicated with open arrowheads. **(d)** Details of Tom-labeled cells in the deeper layers of the OB showing no colocalization with BLBP in the EPL (top), the mitral cell layer (bottom, open arrowhead) and granule cell layer (bottom, filled arrowhead). Scale bar: 10 μm . Similar results were observed in 3 mice.

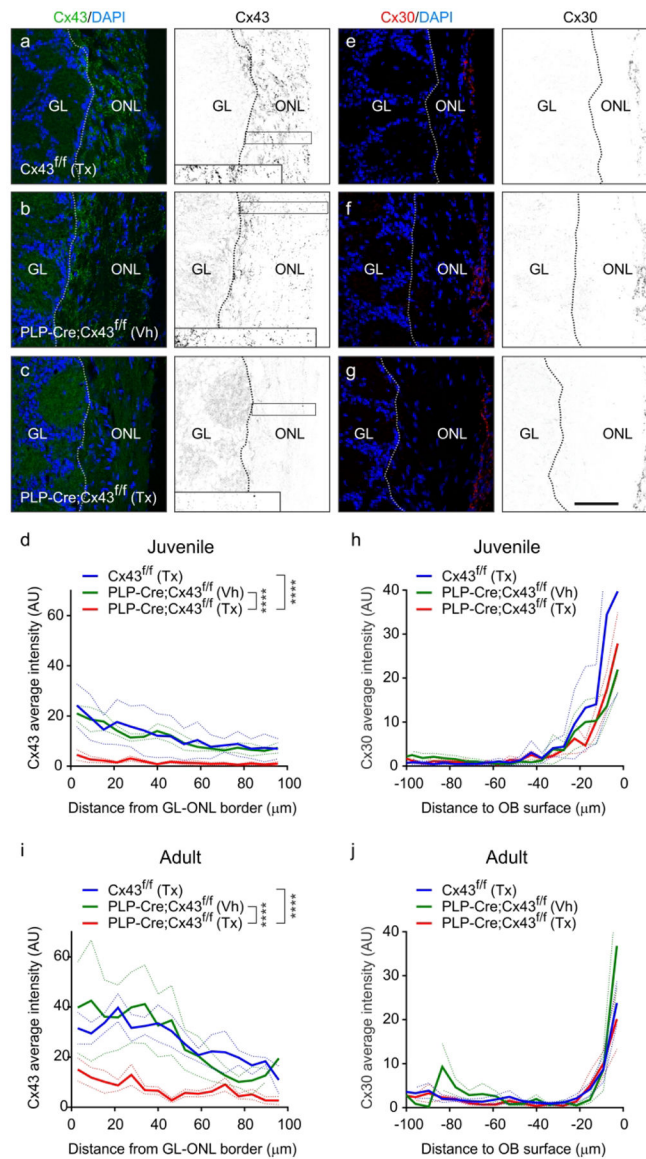


Figure 3. Cre-Lox mediated deletion of Cx43 in olfactory ensheathing cells without upregulation of Cx30.

Representative images of coronal sections of the OB from 1-month-old mice immunostained for Cx43 (green) (a-c) or Cx30 (red) (e-g), corresponding to the following genotypes and treatments received at 2 weeks of age (P14-P19): Cx43^{fl/fl} mouse treated with Tx (a,e), PLP-Cre^{+/-};Cx43^{fl/fl} mouse treated with vehicle (b,f) and PLP-Cre^{+/-};Cx43^{fl/fl} mouse treated with Tx (c,g). Nuclear stain (DAPI) is shown in blue. The transition from the ONL to the glomerular layer is indicated with a dashed line. Images in grayscale correspond to connexin immunoreactivity alone. Rectangular areas correspond to representative regions of interest used for quantification of intensity profiles and are shown in higher magnification as thresholded images at the bottom of corresponding images. Scale bar: 50 μm. (d,i) Average intensity profiles of Cx43 immunolabeling in the ONL as a function of distance from the glomerular layer outer limit for the experimental groups indicated by the labels, at the juvenile (d) and adult (i) stages. (h,j) Average intensity profiles of Cx30 immunolabel in the

ONL as a function of distance to the OB surface for the experimental groups indicated by the labels, at the juvenile (**h**) and adult (**j**) stages. Adult mice were treated with Tx at two months of age (P60-P65). **** $p < 0.0001$, post hoc tests after a significant effect of experimental group and distance in a two-way repeated measures ANOVA (n=3–7 juvenile animals and 4–6 adult animals per group). Dotted lines indicate SEM.

Author Manuscript

Author Manuscript

Author Manuscript

Author Manuscript

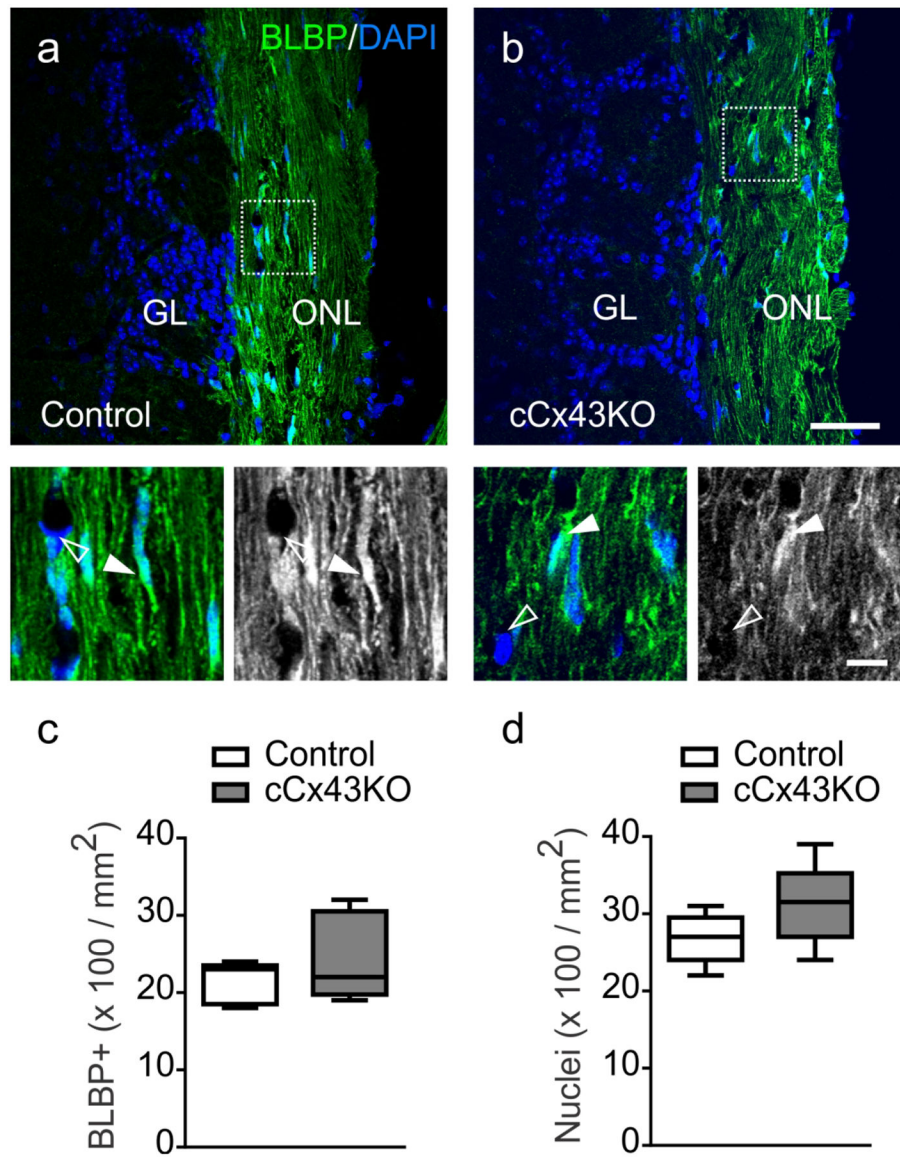


Figure 4. Cx43 deletion preserves the number of olfactory ensheathing cells.

Representative images of OB sections showing immunoreactivity for BLBP (green) and nuclear stain (DAPI, blue) in control (a) and cCx43KO (b) mice. Higher magnifications of the indicated areas are shown below, with the isolated BLBP channel in grayscale. Filled and open arrowheads point at BLBP+ and BLBP- cells, respectively. Scale bar: 50 μ m; inset: 10 μ m. (c,d) Average density of BLBP+ cells (c) and nuclei (d) in the ONL of control and cCx43KO mice (not significantly different, Mann-Whitney test, $p=0.4069$ (BLBP) and $p=0.1104$ (nuclei), $n=5-6$ mice per group).

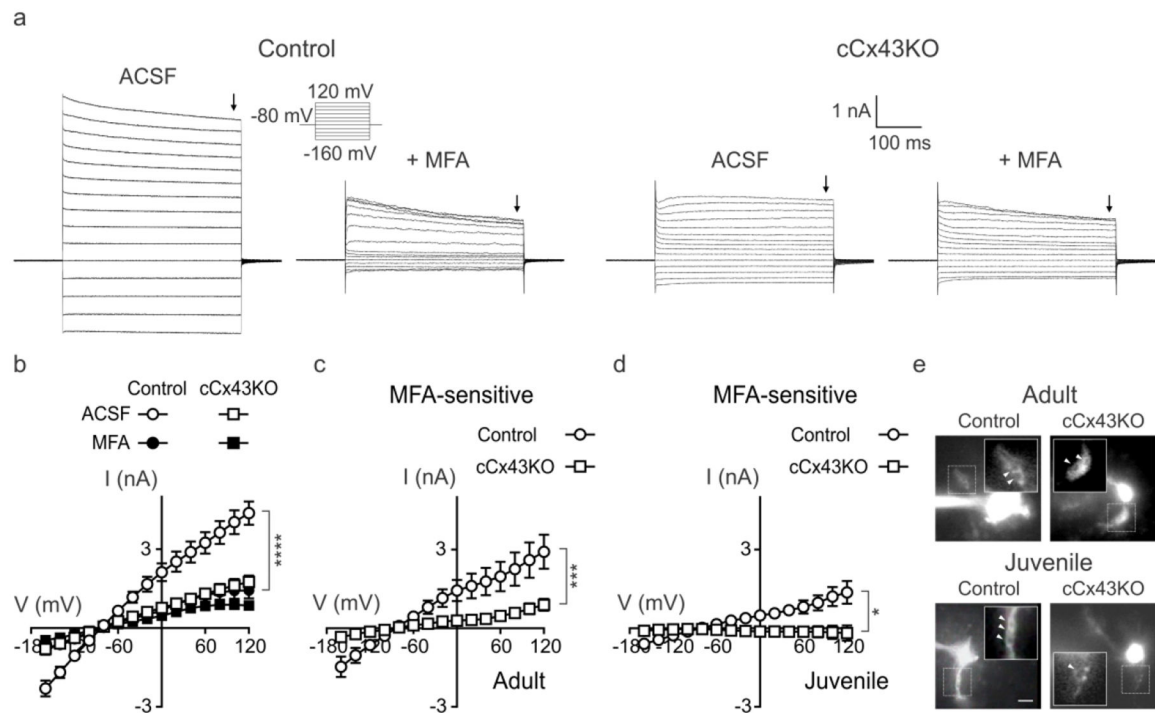


Figure 5. Olfactory ensheathing cells from cCx43KO mice are less sensitive to the connexin blocker MFA.

(a) Representative recordings of OEC whole cells currents evoked by a series of voltage steps (−160 to 120 mV, 20 mV) before and after adding 100 μM MFA in control (left) and cCx43KO (right) mice. **(b)** Average I/V curves measured at the time indicated by the arrows in (a). **** $p < 0.0001$, slopes significantly different after post-hoc tests (Tukey) in two-way ANOVA with experimental group and drug as factors and significant interaction ($p = 0.0032$). Data are mean \pm SEM. **(c,d)** Average I/V curves for the MFA-sensitive current in OECs from control and cCx43KO adult **(c)** and juvenile **(d)** mice. *** $p < 0.001$, * $p = 0.0233$, significant interaction and main effects in two-way repeated measures ANOVA with voltage and experimental group as factors (adults: $n = 5-6$ cells from 4–5 mice per group; juveniles: $n = 3-5$ cells from 3–4 mice per group). **(e)** Representative images of OECs filled with lucifer yellow through the recording pipette, obtained at the end of the recording time to qualitatively identify OECs by their characteristic lacunae (arrowheads in the insets). Scale bar: 10 μm.

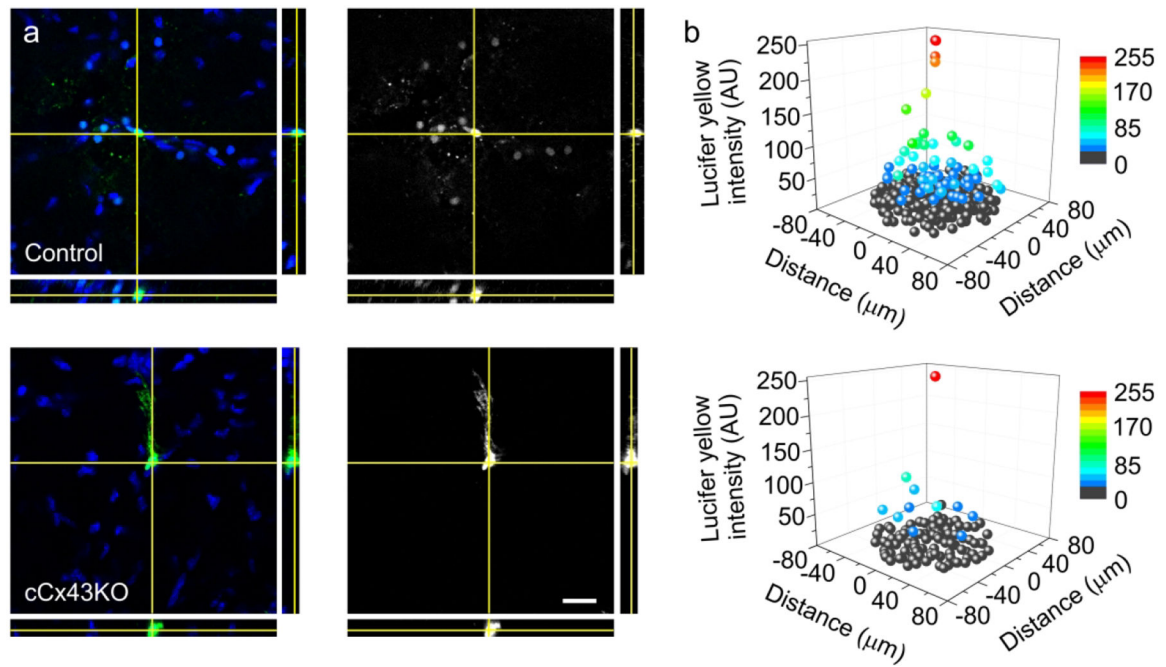


Figure 6. Cx43 mediates gap junction connectivity in olfactory ensheathing cells.

(a) Representative orthogonal projections of image stacks obtained from lucifer yellow (green)-filled OECs from a control mouse (top) and a cCx43KO mouse (bottom). Nuclear stain (DAPI) is shown in blue and the isolated lucifer yellow channel is shown at the right. Scale bar: 20 μm . **(b)** 3D plots showing the relative distance of neighboring nuclei to the dye-filled cell, centered at the origin of the x-y plane, and the lucifer yellow intensity indicated in the z-axis and color mapped (0 to 255 in arbitrary units), for cells from control (top, n=6 cells from 5 mice) and cCx43KO mice (bottom, n=4 cells from 4 mice). Cells considered below threshold for significant dye staining are indicated in gray.

Table 1.

Primary antibodies

Antibody	Host	Antigen	Source	Catalog no.	Dilution (Concentration)
Cx43	Rabbit	C-terminal of 3rd cytoplasmic domain of rat Cx43	Zymed	Cat# 71-0700; RRID: AB_2533973	1:500 (0.5 µg/ml)
Cx43	Mouse	Cx43; synthetic peptide of aminoacids 252-270 (Clone RN26)	Chemicon	Cat# MAB3068; RRID: AB_2110187	1:500 (2 µg/ml)
Cx30	Rabbit	C-terminal of mouse Cx43	Zymed	Cat# 71-2200; RRID: AB_2533979	1:1000 (0.25 µg/ml)
BLBP	Rabbit	GST-tagged recombinant human BLBP	Chemicon	Cat# ABN14 RRID: AB_10000325	1:700 (1.4 µg/ml)
GFAP	Mouse	native GFAP purified from pig spinal cord	Cell Signaling	Cat# 3670 RRID: AB_561049	1:1000 (0.2 µg/ml)